

The effects of rising temperatures on flood quantiles in the Italian Alps can be amplified by different catchment morphologies

Original

The effects of rising temperatures on flood quantiles in the Italian Alps can be amplified by different catchment morphologies / Evangelista, Giulia; Monforte, Irene; Claps, Pierluigi. - In: JOURNAL OF HYDROLOGY. - ISSN 0022-1694. - 662:(2025). [10.1016/j.jhydrol.2025.134014]

Availability:

This version is available at: 11583/3002373 since: 2025-08-08T12:20:29Z

Publisher:

Elsevier

Published

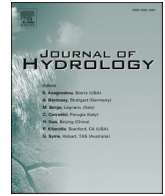
DOI:10.1016/j.jhydrol.2025.134014

Terms of use:

This article is made available under terms and conditions as specified in the corresponding bibliographic description in the repository

Publisher copyright

(Article begins on next page)



Research papers

The effects of rising temperatures on flood quantiles in the Italian Alps can be amplified by different catchment morphologies

Giulia Evangelista^{*} , Irene Monforte, Pierluigi Claps 

Department of Environment, Land and Infrastructure Engineering, Politecnico di Torino, Torino, Italy

ARTICLE INFO

This manuscript was handled by Dr. A. Barrosy, Editor-in-Chief, with the assistance of Svenja Fischer, Associate Editor

Keywords:

Alps
Mountain
Climate change
Flood risk
Elevation

ABSTRACT

This study quantifies potential rates of change in flood quantiles for Alpine basins in Italy under rising temperatures, focusing on the influence of catchment elevation and morphology on natural processes leading to the maximum annual flood. The approach undertaken develops the concepts presented in a previous methodology, that allows to build flood frequency curves by accounting for seasonal variations in the snow-covered portion of the catchment area. We have significantly refined the original methodology by improving the analytical representation of the basin hypsometric curve. This enhanced formulation provides a more accurate characterization of the elevation distribution within catchments, addressing the limitations of the simplified function originally used. This revised approach, named here *FloodAlp*, allows us to systematically assess, for the first time, the role of the basin's hypsometric properties on the sensitivity of current 10-year and 100-year floods to gradual changes of the snowline elevation over a large scale, i.e. the entire Alpine chain of Italy.

Our findings indicate that basins above 2000 m a.s.l. exhibit a pronounced sensitivity to temperature increases, with potential increments of up to 18.5 % and 21 % in the 10-year and 100-year floods, respectively, for a 2 °C rise. A 4 °C increase is found to raise these values by 35 % and 43 %, respectively. A paired-catchment analysis reveals that flood increases due to temperature rise strongly depend on the shape of the elevation distribution: even slight variations in the sinuosity of the hypsometric curve can lead to differences of up to 50 % in the 100-year flood, a finding that would have been missed using the original formulation of the methodology. Given the pronounced morphological heterogeneity of basins in the Italian Alps, the results of this study allow to significantly differentiate, over large areas, flood sensitivity to global warming in mountain basins.

1. Introduction

Flood hazard assessment for hydrological design has traditionally relied on methods that assume a stationary probabilistic analysis of the design flood, based on historical records and regional analyses. In recent years, however, several studies have investigated whether the flood frequency curve of a watershed can undergo changes over time due to climate change, in which case the design procedure should be modified (François et al., 2019). In fact, climate change stands out as a key driver of substantial alterations in flood frequency (Blöschl, 2022). The accumulation of greenhouse gases in the atmosphere has unequivocally caused global warming, with global surface temperature reaching 1.1 °C above 1850–1900 in 2011–2020 (IPCC, 2023). Rising temperatures emerge as a major concern for the vulnerability of mountain regions to the impact of climate change (Wilhelm et al., 2022) as also clearly stated in the IPCC Assessment Report 6 (Adler et al., 2022). Global-scale

analyses comparing observations at lower and higher elevations suggest a remarkable enhancement of warming typically occurring above 500 m above sea level (e.g. Qixiang et al., 2018). Temperature trend analyses reveal that the Alpine region has experienced pronounced warming, averaging an increase of about 2 °C over the period from 1961 to 2020 (Bongiovanni, 2025).

Several studies have highlighted the effects of global warming on mountain hydrology, focusing particularly on the earlier snow melting and shifts in runoff seasonality (e.g. Bavay et al., 2013, Schneeberger et al., 2015, Blahušáková et al., 2020, Hanus et al., 2021, Rottler et al., 2021), variations in the magnitude of winter and summer runoff (e.g. Etter et al., 2017, Moraga et al., 2021, Zexia et al., 2022), as well as changes in the relative contribution of different flood-generating mechanisms (e.g. Chegwiddden et al., 2020, Kemter et al., 2020, Tarasova et al., 2023). Additionally, it has been shown that the complex interplay of glacier retreat and permafrost degradation further

^{*} Corresponding author.

E-mail address: giulia.evangelista@polito.it (G. Evangelista).

<https://doi.org/10.1016/j.jhydrol.2025.134014>

Received 2 April 2025; Received in revised form 25 July 2025; Accepted 1 August 2025

Available online 5 August 2025

0022-1694/© 2025 The Author(s). Published by Elsevier B.V. This is an open access article under the CC BY license (<http://creativecommons.org/licenses/by/4.0/>).

complicates the hydrological dynamics, influencing water availability and flood patterns in mountain basins (Sommer et al., 2020). Therefore, in high-elevation regions, the flood vulnerability might extend beyond areas currently recognized at high risk, and municipalities which were previously subject to “once-in-a-lifetime” events should be aware of the possibility of more recurrent flooding. Castellarin and Pistocchi (2012) observed that the 100-year flood, as estimated from historical hydrological records in Swiss basins, corresponds to a return period of approximately 10 to 30 years when assessed with more recent data. A similar finding was reported by Allamano et al. (2009b) for Switzerland.

The Alps actually deserve special attention, as millions of people live at their foothills and an important fraction of the Italian GDP is produced in this region. In addition, the Alps host about 40 % of Italy’s large dams (Evangelista et al., 2023), i.e. those higher than 15 m or with a storage volume bigger than one million cubic meters. So far, much of the existing research on the effects of climate change on streamflow in high-elevation catchments within the Alps, defined here as catchments with average elevations higher than 1000 m above sea level, has primarily focused on basins in Switzerland (e.g., Köplin et al., 2012, Bavay et al., 2013, Etter et al., 2017, Ragetti et al., 2019, Moraga et al., 2021, Wilhelm et al., 2022) and, to a smaller extent, in Austria (e.g., Meißl et al., 2016, Brunner et al., 2019, Hanus et al., 2021). More fragmented research has focused on the Italian Alps: existing studies cover only relatively small parts of the Italian Alpine basins (e.g., Confortola et al., 2014, Mallucci et al., 2019, Wilhelm et al., 2022, García-Valdecasas Ojeda et al., 2022). Furthermore, not all of the studies cited above investigate the effects of climate change on flood extremes. A comprehensive assessment targeted to floods, that encompasses the entire Italian Alpine chain, is therefore still lacking.

The methodologies employed in the studies cited above predominantly rely on the application of hydrological models, which are often coupled with climate models or integrated with energy budget models to simulate hydrological processes under varying climate conditions. However, these approaches generally require continuous, high-temporal-resolution rainfall data, as well as input variables that are often not easily accessible and may lack reliability, such as solar radiation, wind speed, and cloud cover. Such models, while offering an accurate representation of hydrological processes, need a thorough calibration, which can be particularly challenging in high-elevation catchments and would require stochastic generation of long time series of variables to allow an analysis of extremes.

To try to assess potential effects of global warming on floods across the entire Italian Alpine region using a spatially homogeneous data set and knowledge base, we carry out a simplified, yet comprehensive, analysis of likely rates of change in small and large floods (corresponding to different flood quantiles), with a focus on the role of catchment morphology in modulating these effects. Such an analysis can be of scientific interest while also addressing the practical needs of practitioners concerning engineering design adjustments for climate change. Taking into account the need to increase financial resources to support flood prevention measures (Kundzewicz, 2018), there is a clear need of approaches that can effectively identify the most hazardous sites within a wide area framework. In mountain regions, where elevation and topography strongly influence hydrological processes and where many dams operate from several decades, prioritization can be particularly important.

In our procedure, a simple morpho-climatic conceptual approach is used, i.e. the one developed by Allamano et al. (2009a), and implemented in a model that we name *FloodAlp* here; this model consists in a “derived distribution” for flood frequency (see e.g. Diaz-Granados et al., 1984) and considers the effects of the intra-annual variability of the catchment area covered by snow. The derived distribution model incorporates basic descriptions of the seasonal variation in the freezing elevation, as intersected with the catchment hypsographic curve. Once obtained a baseline frequency curve, future distributions can be generated, for instance, by raising the snowline elevation, allowing for

comparisons between current and future flood quantiles.

Despite Allamano et al. (2009b) applied the methodology to a set of catchments in the Swiss Alps, no validation against current flood frequency curves was performed. While attempting this validation, we have also considered that the original formulation proposed by Allamano et al. (2009a) may in some cases oversimplify the representation of the basin’s elevation distribution, which is a critical element of the methodology. To overcome this limitation, we propose here an alternative formulation of the approach, by implementing an improved parametrization of the area-elevation distribution (hypsometry), thereby improving the representation of diverse hypsometries within such a heterogeneous region.

The key goals of this work are then summarized as follows:

- i. to provide a systematic assessment of how 10-year and 100-year flood quantiles may change with rising temperatures across nearly 200 gauged Alpine watersheds in the Italian Alps, covering a much broader spatial scale than previous studies;
- ii. to investigate the role of basin elevation characteristics and their hypsometric curves on the alteration of flood quantile magnitudes under global warming. To the best of our knowledge, the only study that explicitly examines the influence of basin hypsometry is that of Shea et al. (2021), which primarily focuses on snowpack dynamics rather than directly addressing flood hazard. Moreover, the sample of basins used here has quite distinct characteristics and covers a much wider range of elevations than that investigated in Shea et al. (2021). Later in the paper, further discussion and comparison with the work of Shea et al. (2021) will be presented.

2. Methods

The *FloodAlp* model (from Allamano et al., 2009a) produces flood frequency curves based on a simplified derived distribution methodology, designed to reduce as much as possible the parameters that play a role in the flood-forming conditions in mountain basins. *FloodAlp* reproduces the formation of the maximum annual flood by modeling the complex interactions between the basin elevation distribution, the temperature seasonality and the flood contributing areas, i.e. those subjected to liquid precipitation in each season, where precipitation follows a Poisson-exponential stochastic process. In other words, during a precipitation event, only a portion of the basin is considered “active”, as it lies below the freezing elevation and receives liquid precipitation. In average terms, the freezing elevation $ZT(t)$ varies seasonally, as it follows the thermal regime of an area, reaching its peak in summer and its lowest value in winter. A linear symmetric curve is used to describe the variability of $ZT(t)$ over time (see Fig. 1 in Allamano et al. (2009a)). Because of this variability, the ratio between the flood contributing area and the total basin area varies over time, in a way that depends on the basin hypsometric curve. Here resides the influence of topography in the flood generation mechanism. Runoff is therefore modeled as the sum of two components: direct runoff from net rainfall over the active portion of the basin and snowmelt contribution during the warm season (see Eq. (1) in Allamano et al. (2009a)). Snowmelt is assumed to vary depending on the day of the year and, therefore, on the temperature regime.

To substantially improve the representation of basin hypsometric curves, we have introduced a two-parameter Strahler function, along with an assessment of an effective estimation method. This modification introduces a new parameter into *FloodAlp*’s very limited set of parameters. Given the prompt availability of detailed digital elevation model data, we do not perceive any drawback to this addition. Advantages are instead presented in section 2.1.

The rainfall duration considered here is one day. To preserve the units, the modeled discharge q is a specific daily average discharge, evaluated in mm/d. Model application described in section 3 will better delineate the terms and hypotheses used.

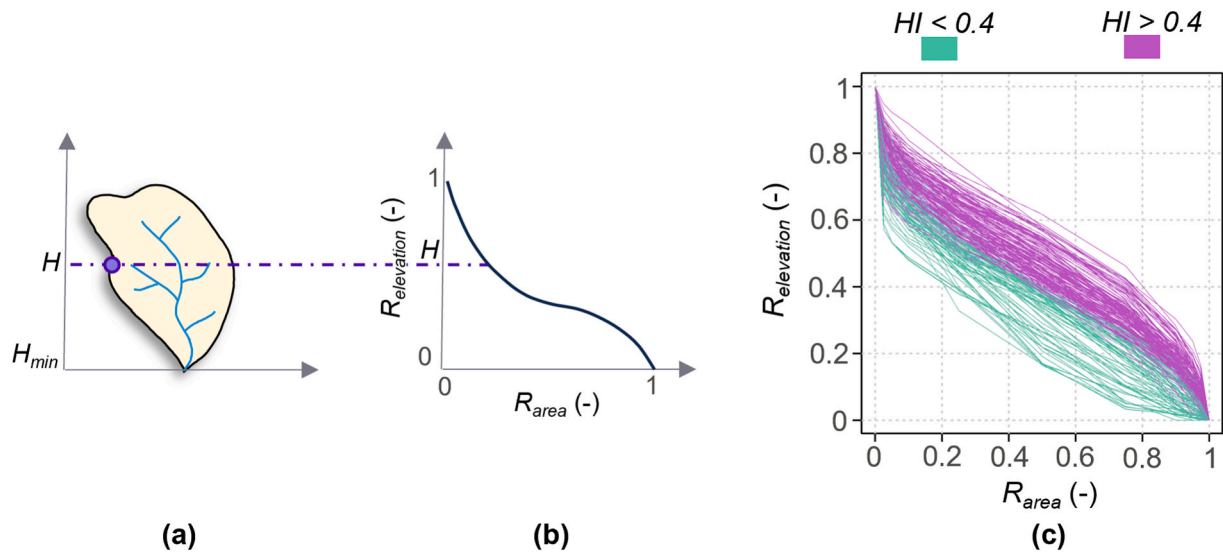


Fig. 1. Simplified representation of a hypsometric curve (a), (b). Empirical hypsometric curves for the sample of 192 basins analyzed (c). Greenish and purple curves correspond to values of the hypsometric integral smaller or larger than 0.4, respectively, according to the Strahler's classification (Strahler, 1952). H = elevation; H_{min} = minimum basin elevation; $R_{elevation}$ = relative elevation; R_{area} = relative area; HI = hypsometric integral.

2.1. An improved parametrization of the hypsometric curve

As mentioned in the previous section, the watershed hypsometry plays a primary role in the way the *FloodAlp* model works. The shape of the hypsometric curve influences the extent of the area that directly contributes to flood formation for a given reference temperature (see Allamano et al. (2009a) for further details). In its original formulation, the methodology underlying the *FloodAlp* model entails parametrizing the hypsometric curve using a simplified one-parameter function:

$$R_{elevation} = \frac{H - H_{min}}{H_{max} - H_{min}} = \frac{f_c(t)}{1 + \xi(1 - f_c(t))} \quad (1)$$

where the left hand side term represents the normalized watershed elevation; $f_c(t)$ is the normalized contributing area, i.e. the ratio between the portion of the basin that contributes to surface runoff in a given time and the total basin area; ξ controls the flexure of the hypsometric curve and assumes only values greater than -1 . A graphical representation of $R_{elevation}$ is given in Fig. 1a and 1b. The area under the curve, which represents the hypsometric integral, would yield the same value whether calculated using the 1-parameter representation of the empirical hypsometric curve given in Eq. (1) or derived from a digital elevation model (see Pike and Wilson, 1971). However, the 1-parameter fitting curve and the empirical one may differ substantially in terms of shape: Fig. 1c shows the variability of the empirical hypsometric curves for the sample of 192 basins analyzed in this study. A first category of basins (purple curves) exhibits concavity in the summit portion and convexity in the end portion (double curvature) and a hypsometric integral $HI > 0.4$ (Strahler, 1952). On the other hand, a second family of curves (greenish curves) shows a general upward concavity (single curvature) and reduced values of the hypsometric integral. Notably, 126 basins have an HI value above 0.4, with 28 of them exceeding 0.5.

Only the second shape category can be adequately represented by a single-parameter function. Therefore, we looked for an alternative parametrization of the hypsometric curve that would be able to capture even the double curvature shapes. We then evaluated the improvements gained by including an additional parameter in the procedure. The function adopted and implemented in the model is the one proposed by Strahler (Strahler, 1952):

$$y = \left(\frac{1 - x - x_0}{x + x_0} \right)^z \quad (2)$$

where x_0 and z control the HI value and the degree of sinuosity of the curve, respectively. Specifically, so-called "S-shaped" curves are characterized by z values < 1 ; z values > 1 , on the other hand, identify curves with a single upward concavity. x_0 and z are estimated iteratively by nonlinear least squares optimization. The relative differences between the empirical hypsometric integral and that estimated from the curve modeled using Eq. (2) are very small, with a median value of -0.048% and a mean value of -0.045% . In our analysis, we also explored a 3-parameter hypsometric curve formulation based on Strahler's function (e.g. Bajracharya and Jain, 2021) that enables a more precise alignment of the function with the initial and final curvature of the hypsometric curve. Of course, this model offers an even closer fit to the empirical curve. Nevertheless, we decided that the two-parameter formulation struck a well-balanced compromise between approximation accuracy and the simplicity of parameter estimation. The results of adopting the two different formulations (i.e. 1-parameter and 2-parameter) for two example basins, the Chisone at Fenestrelle ($HI = 0.48$) and the Galambra at presa centrale Chiomonte ($HI = 0.58$), are shown in Fig. 2. Fig. 2a and 2b show the goodness of interpolation of the empirical quantiles of the hypsometric curve by the one- (in red) and two-parameter (in blue) formulations.

Different parametrizations of the hypsometric curve directly affect the behavior of the $f_c(t)$ factor and, consequently, influence the flood frequency curve generated by the model. For instance, one can notice from Fig. 2c that, in the case of the Chisone at Fenestrelle basin, the two-parameter formulation yields a higher percentage of contributing area during the warm season, and a reduction during the winter. These differences become negligible when the double curvature assumed by the hypsometric curve is lost (Fig. 2d). Moving on to the model outcomes, the two-parameter hypsometric function yields higher specific discharge values for the same return period compared to those derived from the simplified one-parameter formulation, i.e. the new formulation adopted is found to be safety-oriented. Consistently with what observed in Fig. 2c and 2d, the frequency curves obtained from the two configurations exhibit a pronounced difference in the case of the Chisone at Fenestrelle basin (Fig. 2e), whereas they completely overlap for the Galambra at presa centrale Chiomonte basin (Fig. 2f).

2.2. Model validation

The *FloodAlp* model allows to derive a flood frequency curve (FFC)

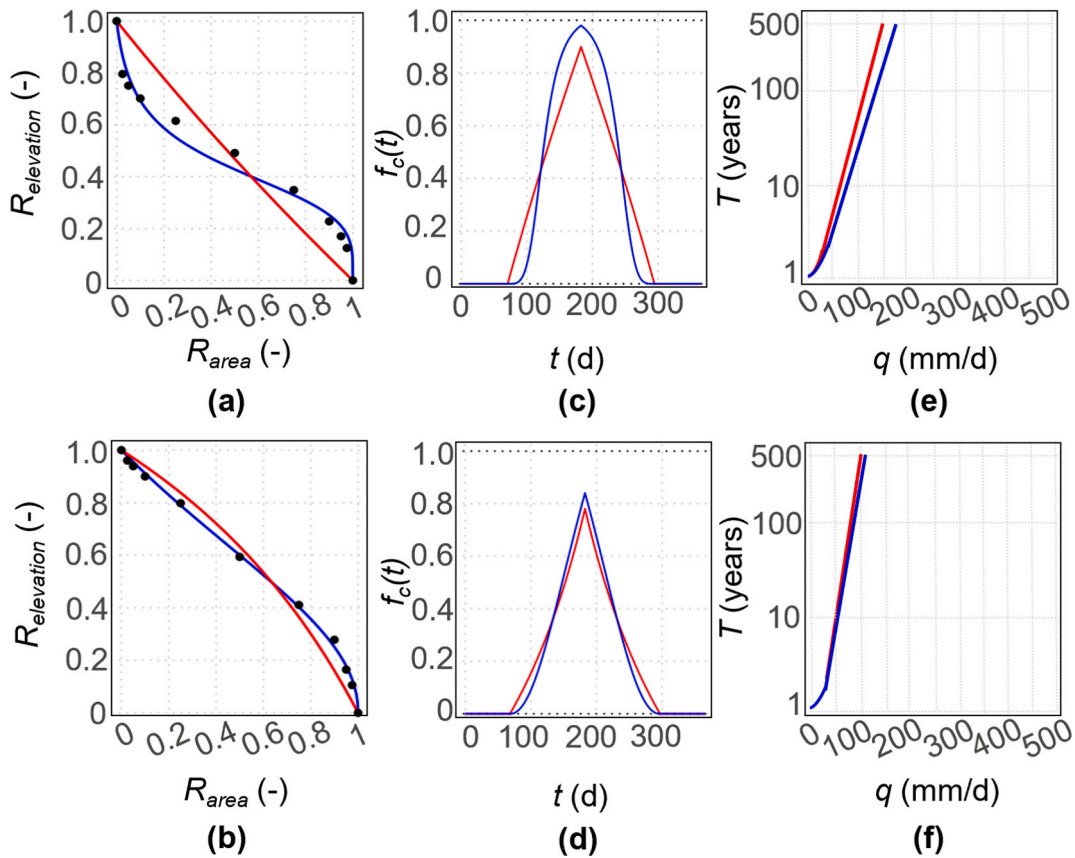


Fig. 2. Differences between the original hypsometric curve formulation (in red) and the two-parameter formulation (in blue) in terms of: goodness of interpolation of the empirical quantiles of the hypsometric curves (a), (b); temporal evolution of the normalized contributing area (c), (d); flood frequency curves (e), (f). Figures in the first line refer to the Chisone at Fenestrelle basin, those in the second line to the Galambra at presa centrale Chiomonte basin. $R_{elevation}$ = relative elevation; R_{area} = relative area; $f_c(t)$ = normalized contributing area; t = time; T = return period; q = specific daily average discharge.

analytically from a rainfall frequency curve (RFC). As mentioned in the Introduction, the model is explicitly implemented here, for the first time, over different river basins to generate FFCs. The quality of fitting is then quantitatively assessed. As illustrated in Fig. 3, which shows the model application for an example basin, *FloodAlp* reproduces the shape of the FFC, apart from a scaling factor, represented by the runoff coefficient C in Eq. (1) of Allamano et al. (2009a). In Fig. 3, the dotted blue curve is first obtained using $C = 1$. By multiplying the dotted curve by a $C \neq 1$, one obtains the solid blue curve. The runoff coefficient C can be then regarded as an indicator of the extent of the adjustment needed by the model's curve to match the observed q values: the smaller the C value, the greater the adjustment required. A second interpretation can also be considered: the dotted blue curve in Fig. 3 represents the FFC which derives from the RFC only after accounting for the partial contributing area effect due to snow accumulation. The solid blue curve, on the other hand, incorporates a further reduction, caused by infiltration losses, through the proportional coefficient C .

To test the effects deriving from snow accumulation and melting on the FFC, one can quantify the extent of deviation between a given precipitation quantile and the corresponding flood quantile recorded on the curve built with $C = 1$ (hereinafter Δq_1). In the same way, the distance between the flood quantiles measured on the $C = 1$ and $C \neq 1$ curves for the same return period (hereinafter Δq_2) can be calculated. Considering a reference return period T , one can then define:

$$\Delta q_1 = q_{T,rainfall} - q_{T,flood,C=1} \quad (3)$$

and

$$\Delta q_2 = q_{T,flood,C=1} - q_{T,flood,C \neq 1} \quad (4)$$

To use a $C \neq 1$, its value has to be calibrated somehow. One possible approach is to search for a value that ensures that the flood frequency curve produced by the model crosses the point corresponding to the maximum observed specific discharge. Alternatively, calibration could be performed by forcing the $C = 1$ FFC to pass through a set of n randomly selected points on the empirical curve.

Since this study does not aim to estimate flood quantiles for specific return periods, but rather to assess the magnitude of their variation induced by global warming, all analyses are carried out by using $C = 1$ for all the watersheds. Setting $C = 1$ essentially means we are treating the specific discharge q as a basin inflow, before it undergoes the conversion into runoff. This allows us to focus exclusively on temperature-driven effects on flood quantiles. Within the model framework, this assumption does not affect the magnitude of changes in flood quantile values due to global warming: variations in the FFC due to climatic perturbations remain independent of C and its association with the rainfall-runoff conversion process, as C works solely as a scaling factor. Investigations on the variability of the runoff coefficient are therefore postponed to future developments.

However, to give the reader an indication of the model's performance in reproducing the shape of the empirical FFCs, C values calibrated by adjusting the model so that the FFC produced crosses the point corresponding to the maximum observed specific discharge are reported in section 5.1. To quantitatively investigate the model's accuracy in reproducing the form of the empirical flood frequency distributions, the Kolmogorov-Smirnov distance (KS_d) is used. KS_d is computed as follows:

$$KS_d = \max |F(x_i) - \Phi(x_i)| \quad (5)$$

where $F(x_i)$ and $\Phi(x_i)$ represent the simulated cumulative

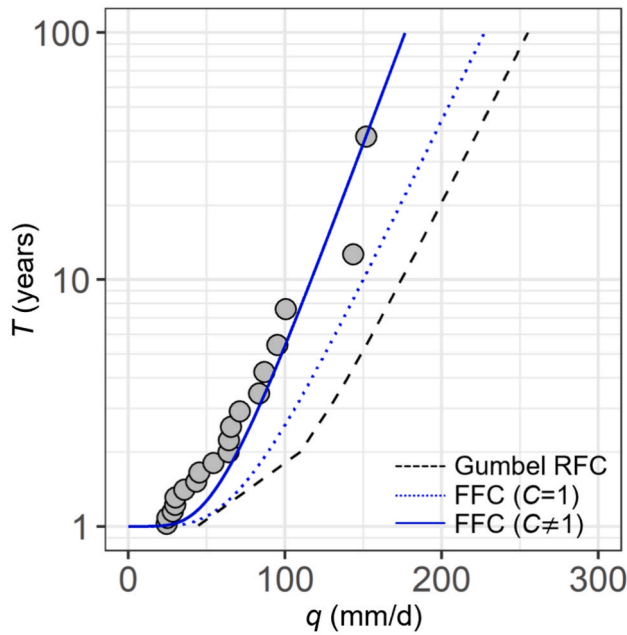


Fig. 3. Example of flood mitigation induced by snow modeled with *FloodAlp* for an example basin in the Italian Alps. Dotted and solid blue lines show flood frequency curves (FFCs) obtained using a runoff coefficient $C = 1$ or $C \neq 1$, respectively. Curves are compared to the annual maxima of daily discharges observed at the same station. The dashed black line is the Gumbel rainfall frequency curve (RFC), obtained as the annual maximum of the Poisson-exponential process.

probability and the empirical one computed at the observed sample value x_i , respectively.

2.3. Introduction of climate variations

According to the model framework, one can recognize that an increase in temperature over time would distort the FFC of a mountain basin, causing a shift in its slope (see Allamano (2008)). The magnitude of a specific flood quantile, as determined from the “future” curve, will differ from the same quantile under present conditions in a measure that depends on the distance between the two curves. To investigate this effect and to evaluate whether warming differentially impacts small and large floods, we analyze two reference quantiles associated with return periods of 10 and 100 years, hereafter referred to as q_{10} and q_{100} , respectively. q_{100} has been chosen, here as it represents a standard metric used for infrastructure design.

To figure out the range of potential changes in the current 10-year and 100-year flood quantiles in the Alpine basins of Italy, we assume a generalized temperature increase by rigidly shifting the thermal regime in the model by an amount ΔZT . The temperature lapse rate within the Alps typically varies between 5°C and 7°C per 1000 m of elevation (e.g. Rolland, 2003, Scherrer et al., 2021, Avanzi et al., 2023). A constant in time and uniform in space lapse rate of $6.5^\circ\text{C}/1000\text{ m}$ is adopted in this study, following standard practice in the literature. By considering gradually more severe increments in the average annual temperature, from $+1.5^\circ\text{C}$ to $+4^\circ\text{C}$ (consistent with those identified by the Intergovernmental Panel on Climate Change), the snowline regime curve is gradually shifted upward of about 150 m for each 1°C increase.

The rate of change of the current estimate of the two selected quantiles has been then computed as:

$$\Delta q_{10} = \frac{q_{10, \text{future}} - q_{10, \text{current}}}{q_{10, \text{current}}} \times 100 \quad (6)$$

and

$$\Delta q_{100} = \frac{q_{100, \text{future}} - q_{100, \text{current}}}{q_{100, \text{current}}} \times 100 \quad (7)$$

where $q_{10, \text{future}}$ and $q_{100, \text{future}}$ are computed by considering temperature increments of 1.5°C , 2°C , 3°C and 4°C . It is important to clarify that these increments should be regarded as referring to the time frame in which the model parameters have been estimated.

2.4. Investigation of the role of the basin's hypsometric properties

In order to assess the impact of the basin's hypsometric characteristics on its sensitivity to rising temperatures, the concept of paired-catchment approach (e.g. Folton et al., 2015, Ochoa-Tocachi et al., 2016, Kreibich et al., 2017) is used. Catchment pairs are created and sorted to identify cases which are as similar as possible in selected key catchment attributes, but rather different in their rate of increase of flood magnitudes. For all possible pairs of catchments, the n-dimensional Euclidian distance between their main features is calculated ($d_{\text{attributes}}$, see Eq. (8)), as well as the absolute value of the difference between their rate of increase of q ($d_{\Delta q}$, see Eq. (9)):

$$d_{\text{attributes}} = \sqrt{\sum_{i=1}^n (r_i - s_i)^2} \quad (8)$$

$$d_{\Delta q} = |\Delta q(r) - \Delta q(s)| \quad (9)$$

where r and s are the two catchments in the pair and i denotes a generic catchment feature. The paired-catchment approach is adopted to try to highlight disparities between basins in terms of their hypsometric features, i.e. z and x_0 . Therefore, the following attributes have been selected to compute $d_{\text{attributes}}$: i) basin area, ii) minimum and mean basin elevations, and iii) catchment-averaged mean total precipitation per year, while a temperature increase scenario of 2°C is used to calculate $d_{\Delta q}$. To identify which catchment pairs to investigate among all the possibilities, we sort the basin pairs based on the ratio $d_{\text{attributes}}/d_{\Delta q}$, from smallest to largest. This process returns pairs that exhibit similarity in their catchment attributes but display considerable variations in their rate of increase of q .

3. Study area and data

The study area includes the Italian Alpine region and encompasses a total of 192 watersheds for which hydrologic data are available. The overall area is shown in Fig. 4. Watersheds were selected based on two criteria:

- the mean elevation must exceed 1000 m a.s.l.;
- a minimum of 10 years of recorded annual maxima of daily discharges must be available. The choice to use daily discharges lies in the greater availability of this type of data with respect to peak flow data; additionally, they are aligned with the rainfall data (elaborated from Pavan et al., 2019) adopted for building the flood frequency curves. Furthermore, working with daily rainfall and discharge data allows us to avoid defining a critical duration for each catchment, something that couldn't remain constant but would need to be adjusted day by day according to the changing extent of the contributing area. This would considerably increase the model's complexity.

Discharge data, updated to 2022, are collected in the *Catalogo delle Piene dei Corsi d'acqua Italiani* (Claps et al., 2025), the most recent systematic collection of extreme floods in Italy.

The area we investigate spans over 20,000 square kilometers and extends approximately 500 km horizontally, exhibiting substantial

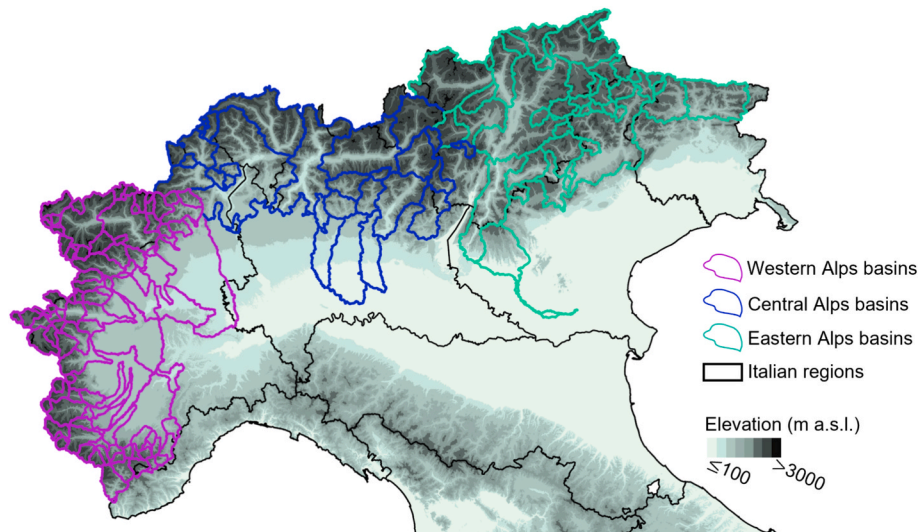


Fig. 4. Elevation of the study area and basin boundaries, grouped by geographical regions.

variability in basin characteristics. Based on just geography, the study area can be classified into three geographical regions: western Alps (encompassing 114 basins), central Alps (encompassing 35 basins) and eastern Alps (encompassing 43 basins), as depicted in Fig. 4. While not directly based on a cluster analysis, the adopted subdivision can be useful for recognizing variations in catchment characteristics across such a broad region. The dataset exhibits a wide range of geomorphoclimatic features: as shown in Table 1, small and high in elevation basins are more prevalent in the western region. The largest basins, with the lowest elevation outlets, are located in the central Alps, within the regions of the Adda, Po, and Ticino rivers. Furthermore, notable differences exist in rainfall regimes, as the mean value of the total amount of precipitation per year ranges from about 1000 mm to 1700 mm.

The parameters used to systematically apply the model over the whole dataset are as follows: i) the freezing-curve boundaries ZT_{max} and ZT_{min} , i.e. the range within which the thermal regime varies, on average, in one year; ii) the parameters of the fitted hypsometric curve, together with the maximum and minimum basin elevations; iii) the mean total annual precipitation, spatially averaged over the basin; iv) the catchment-averaged values of the α and λ parameters of the Poisson-exponential model of precipitation: α is the average of the annual maximum rainfall intensity (mm/d) and λ is the average rate of storm occurrences per year (y^{-1}). As rainfall events are Poisson-exponentially distributed, the CDF (cumulative distribution function) of precipitation follows a Gumbel distribution (e.g., Madsen et al., 1997) and α and λ

Table 1

25th, 50th, and 75th quantile values of basin areas, characteristic elevations and catchment-averaged mean total annual precipitation for the western, central, and eastern Alps. Area = catchment area; H_{min} = minimum basin elevation; H_{max} = maximum basin elevation; H_{mean} = mean basin elevation; MAP = catchment-averaged mean total annual precipitation.

Region	Quantile (%)	Area (km ²)	H_{min} (m a.s.l.)	H_{max} (m a.s.l.)	H_{mean} (m a.s.l.)	MAP (mm)
Western Alps	25	77	385	2698	1508	953
	50	180	703	3304	1896	1078
	75	576	1204	3756	2259	1211
Central Alps	25	77	198	2990	1292	1297
	50	395	255	3337	1673	1435
	75	1681	930	3886	2122	1662
Eastern Alps	25	127	313	3077	1624	954
	50	282	792	3180	1834	1102
	75	895	1058	3437	1935	1276

are analytically related to the distribution parameters.

The freezing elevation has been assumed to range between 0 and 3000 m a.s.l., based on the thermometric regimes of 300 stations belonging to the database used by Claps et al. (2008). The mean annual precipitation has been averaged within each basin by processing monthly mean rainfall maps from 1951 to 2021, produced by Braca et al. (2021).

To compute catchment-averaged values for the rainfall parameters α and λ of the Poisson-exponential model, a gridded database of daily rainfall depths throughout the Alps was needed. To this end, daily gridded rainfall depths at a 5-km resolution (Pavan et al., 2019) have been used. These data were built using time series of daily precipitation measured from 1961 to 2015 by a climatological monitoring network held by Regional Meteorological Services and/or Regional Functional Centers of the political regions involved, as Piemonte, Lombardy, Veneto, Trentino Alto Adige and Friuli Venezia Giulia. Starting from the maps produced by Pavan et al. (2019), which are available in netCDF format, we have extracted maps of daily annual maxima of rainfall depths and computed the average values of α and λ .

4. Results

4.1. Relative changes in the 10-year and 100-year flood quantiles under rising temperatures

Current and potential future FFCs have been produced with the model *FloodAlp* for various temperature scenarios, on the whole set of 192 basins in the Italian Alps. In particular, future FFCs have been built by running the model with $ZT(t)$ curves shifted according to the expected temperature increments.

Given the coverage of the entire Alpine chain in Italy, we have examined the spatial patterns of variability of Δq_{10} and Δq_{100} values to possibly recognize the influence of macroscopic morphological features on the results. The outcomes, presented in Fig. 5, are organized according to the main catchments within the study area, as illustrated in Fig. 5a. Boxplots with gray borders represent results from the least severe scenario (+1.5 °C), while the black line boxplots refer to those deriving from the most severe scenario (+4°C). For both scenarios, Δq_{10} values (Fig. 5b) are consistently greater than zero, with the sole exception of the Stura di Viù at Lago della Rossa catchment, within the Stura di Lanzo river basin. A consistent increase in 100-year return period flood quantile values due to increased temperature can be found everywhere. Both Δq_{10} and Δq_{100} values increase with the severity of the scenario considered. Overall, the growth rate of Δq_{100} remains

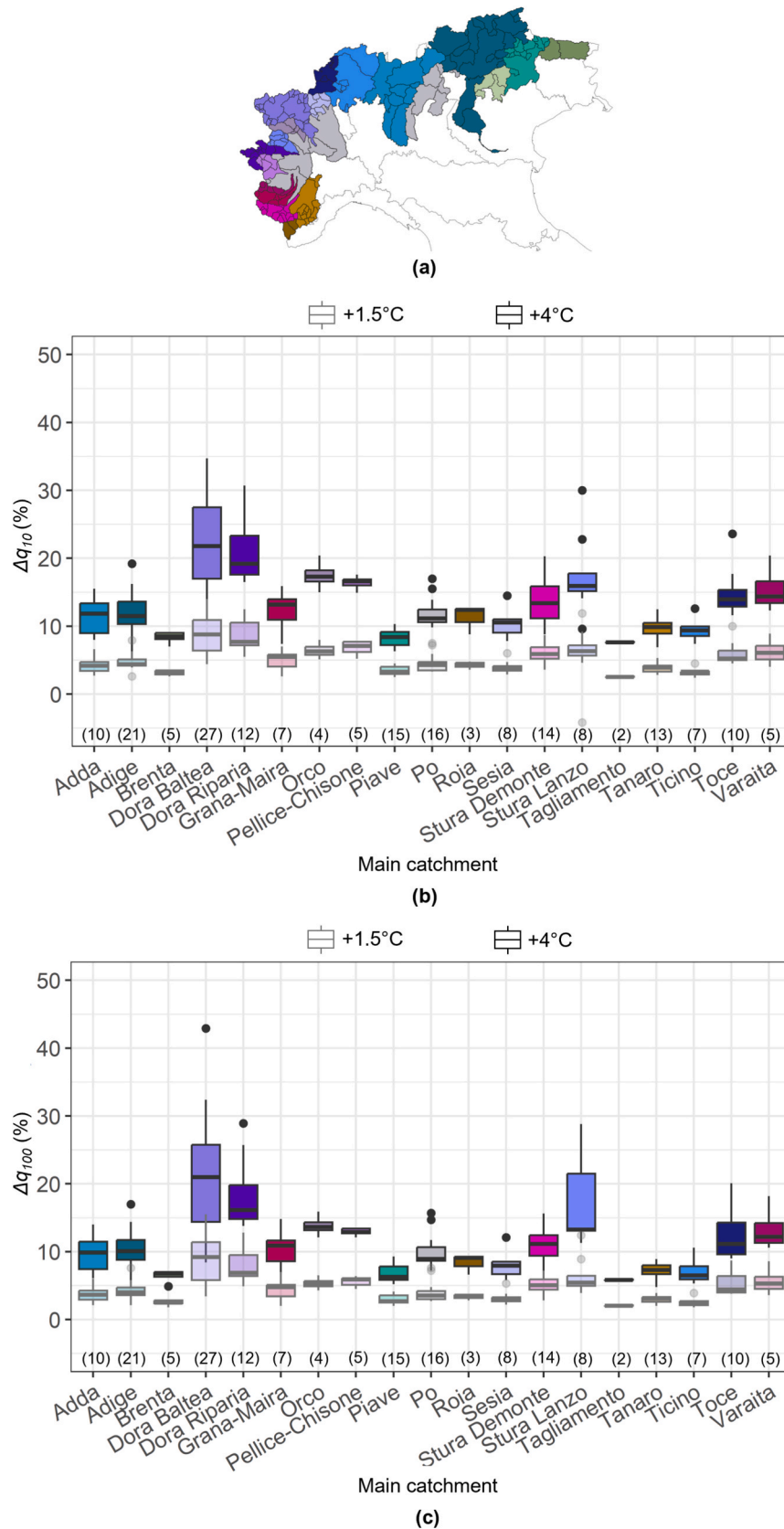


Fig. 5. Model results. 192 basins investigated grouped by main catchments (a); percentage increase in flood quantiles with 10-year return period (Δq_{10}) for a temperature increase of 1.5 (gray line boxplots) or 4 degrees (black line boxplots) (b); percentage increase in flood quantiles with 100-year return period (Δq_{100}) for a temperature increase of 1.5 (gray line boxplots) or 4 degrees (black line boxplots) (c); Numbers in brackets indicate how many basins are included in each main catchment.

consistent across the different scenarios with increasing severity, as we move to $\Delta T = 4^\circ\text{C}$. Looking at Fig. 5b and 5c, exceptions are found within the Orco and the Pellice-Chisone catchments, where wider gaps between $\Delta q_{+1.5^\circ\text{C}}$ and $\Delta q_{+4^\circ\text{C}}$ values are noticed.

A pronounced spatial variability is observed in both Δq_{10} and Δq_{100} values, with some geographical coherence. For a 4°C rise, Δq_{10} ranges from 7 % to 35 % in the western Alps, while the maximum increase in the eastern Alps is 19 %. Similarly, Δq_{100} varies from 5 % to 43 % in the western Alps, with the maximum increase in the eastern Alps reaching 17 % under the same temperature scenario.

The rate of increase in the 10-year flood for each scenario is generally higher compared to the 100-year flood. A few exceptions can be found within the Dora Baltea, Stura di Lanzo and Toce main catchments, in the western and central Alps. Further detailed analysis of these exceptions will be presented in the Discussion section.

As an example, in the Supplementary Material (Figs. S1 to S19) the reader can find plotted bundles of current and future FFCs (for a $+2^\circ\text{C}$ scenario), grouped by main catchments.

4.2. Primary factors affecting changes in flood quantiles

To further investigate the spatial variability of Δq_{10} and Δq_{100} , Spearman's rank correlation coefficients have been computed between these flood quantile changes and basin morphological, hypsometric, and climatic characteristics. In Fig. 6, the correlation matrices for the variables listed in section 3 are shown for the three geographical regions identified. For the sake of clarity, only results for Δq_{10} are represented in Fig. 6, but similar results are found also for Δq_{100} .

Overall, mean basin elevation stands out as the primary factor influencing the increase in flood magnitude, in line with findings from previous studies (e.g. Köpflin et al., 2012, Muelchi et al., 2021). In fact, as basin elevation rises, the time interval during which precipitation falls as snow increases. Slightly less pronounced, also minimum basin elevation proves to be a significant predictor variable in the western Alps.

In the case of the western Alps (Fig. 6a), the parameter that controls the shape of the hypsometric curve (z) shows to contribute to explain some of the spatial variability in Δq_{10} across all scenarios. Notably, a negative correlation is observed with rising temperatures. This means that as z decreases, i.e., as the portion of the area at higher elevations increases, the change in the 10-year flood quantile becomes more significant. This relationship and its implications will be explored in detail

in the following sections.

Hypsometry does not seem to exert such a significant influence in the central and eastern Alps (Fig. 6b and 6c), where mean and maximum elevations remain the dominant morphological factors. To ensure that this result is not affected by differences in the data sample characteristics across the three sectors (see Table 1), we carried out analyses to examine how pairs of morphological parameters (x_0 and z) are distributed across basins in the western and eastern sectors of the Alps. The results indicate that these parameter pairs exhibit considerably greater variability in the western Alps compared to the eastern sector. Furthermore, we found that the $x_0 - z$ values are independent of basin size. This finding supports the idea that the significance of the hypsometric curve on the Δq values observed in the western Alps is driven by morphological differences between these basins and those in the eastern sector, regardless of their generally smaller size.

Interestingly, while minimum basin elevation appears to be a reasonably reliable predictor for changes in flood quantiles in the western Alps, its correlation is definitively weaker in other regions. This difference may be attributed to the generally lower elevations of basin outlets in the central and eastern Alps compared to those in the western region (see Table 1).

Fig. 7 shows the relationship between Δq_{100} and the basin mean elevation for a scenario of 2°C temperature increase. Triangles identify catchments upstream of large dams. Looking at Fig. 7, it can first be seen that several basins upstream of dams are among those experiencing the largest increases in the 100-year flood quantile. This can be well understood if considering that dams are typically located at very high elevations. This evidence draws attention to the need to account for the role of snow in hydrological modeling of basins in the presence of reservoirs in the Italian Alps. Evaluating the potential for increased flood peaks due to temperature increases is likely to be crucial to keep hydrological safety assessments of dams up-to-date.

Starting from mean elevations higher than about 2000 m a.s.l., the variability of Δq_{100} for similar catchments looks more pronounced compared to lower elevations. As an example, one can consider the Chisone at Fenestrelle (basin ID = 39) and Galambra at presa centrale Chiomonte (basin ID = 75) basins, previously used as examples in Fig. 2. Although they share very similar features (see Table 2 in the following section), their Δq_{100} values differ by a factor of two, with values of 8 % for Chisone at Fenestrelle and 17 % for Galambra at presa centrale Chiomonte. A deeper investigation of the impact of hypsometric characteristics using a paired-catchment analysis is described in the

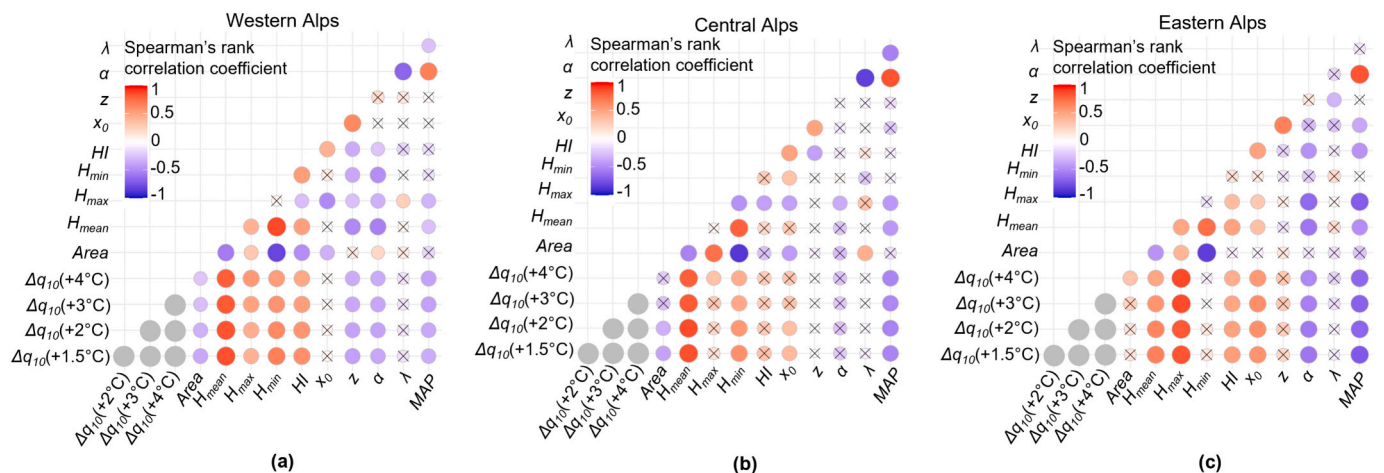


Fig. 6. Spearman's correlation coefficients between the percentage increase in flood quantiles with 10-year return period (Δq_{10}) and the influencing factors for western (a), central (b) and eastern (c) Alps. Crosses refer to non-significant correlations at the 5 % level. Correlation coefficients between different Δq_{10} values are not reported numerically (gray points in the lower left corners of the correlation matrices). Area = catchment area; H_{mean} = mean basin elevation; H_{max} = maximum basin elevation; H_{min} = minimum basin elevation; HI = hypsometric integral; x_0 = Strahler function coefficient; z = Strahler function exponent; α = catchment-averaged average daily extreme rainfall; λ = catchment-averaged rate of storm occurrences per year.

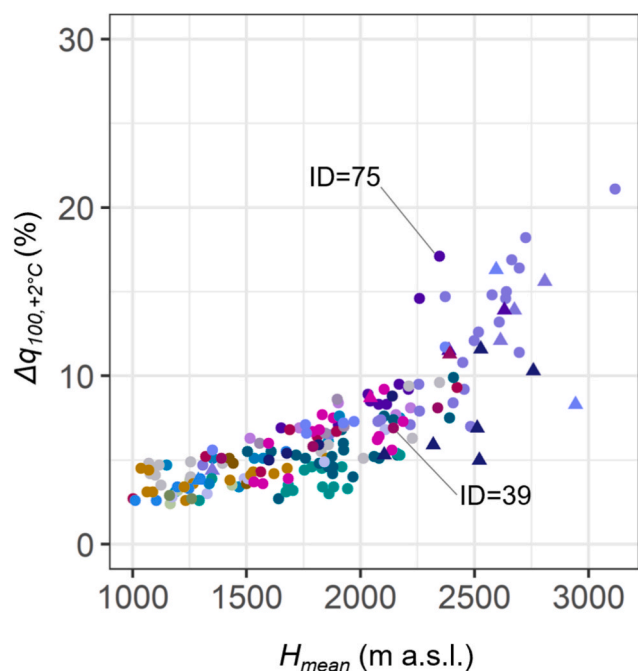


Fig. 7. Percentage increase in flood quantiles with 100-year return period (Δq_{100}) as function of mean basin elevation (H_{mean}) due to a 2 °C temperature increase. Triangles indicate basins upstream of large dams. Main catchments are color-coded as in Fig. 5a. Chisone at Fenestrelle (ID = 39) and Galambra at presa centrale Chiomonte (ID = 75) basins are highlighted.

following section.

4.3. Influence of the basin's hypsometric properties

q_{100} is considered first to compute the ratio $d_{attributes}/d_{\Delta q}$, following the procedure described in section 2.4. Among all the identified pairs of most similar basins, five of them are further selected to highlight the local influence of hypsometric characteristics. Their results are presented in Fig. 8, and their main features are given in Table 2. Consistently with what was observed in Fig. 6, four out of the five relevant case studies are located within the western Alps. Only one, that encompassing the Toce basins (pair n.5), is located within the central Alps, very close to the boundary with the western Alps, while no relevant cases have been identified in the eastern Alps. All these basins have a mean elevation higher than 2000 m a.s.l., confirming that hypsometric features exert a growing influence as elevation increases.

Among the five selected cases, three main categories emerge.

Table 2

Key characteristics of the selected paired catchments. Basin IDs are given in Table S1 in the Supplementary Material. HI = hypsometric integral; MAP = mean value of the catchment-averaged total annual precipitation; Δq_{100} = percentage increase in flood quantiles with 100-year return period.

Pair N°	Category	Basin ID	Area (km ²)	Mean elevation (m a.s.l.)	Minimum elevation (m a.s.l.)	Maximum elevation (m a.s.l.)	Empirical HI (-)	MAP (mm)	Δq_{100} (%)
1	C	39	153.5	2155	1152	3232	0.48	844	8
		75	15.8	2346	994	3321	0.58	908	17
2	A	133	41.2	2608	1610	3447	0.54	962	13
		141	81.1	2696	1644	4006	0.44	952	17
3	A	52	92.8	2613	1697	3694	0.46	928	12
		60	70	2663	1713	3565	0.51	974	17
4	B	29	27.7	2449	1785	3083	0.51	1182	11
		36	22.7	2483	1777	3213	0.49	1202	7
5	C	180	5.2	2527	2217	3508	0.24	1395	12
		183	11.8	2512	2151	3184	0.34	1419	7

Category A encompasses basins characterized by nearly parallel hypsometric curves. Despite exhibiting the same degree of sinuosity, these curves differ in the value of the hypsometric integral (i.e., the area under the curve). Basins of pairs number 2 (ID = 133 and ID = 141) and number 3 (ID = 52 and ID = 60) fall into this class. On the other hand, basins belonging to category B (for instance, basins with ID = 29 and ID = 36 in pair number 4) exhibit hypsometric curves with very similar values of the subtended areas, but different degrees of sinuosity. It is important to note that in this second case the original formulation of the methodology adopted, which involves 1-parameter hypsometric curve modeling (see Eq. (1)), would not have been able to detect any difference between the watersheds. Differences in terms of the hypsometric integral alone, on the other hand, would have been identified even using the original 1-parameter formulation.

Finally, intermediate situations (category C) are represented by the basins in the remaining pairs. In particular, in the cases number 1 and 5, there exists a discrepancy not only in the value of the hypsometric integral and the level of sinuosity, but also in the double-concavity curve versus a single-concavity upward (pair number 5) or downward (pair number 1) curve.

Table 2 reveals that the most substantial disparities in the rate of change of q_{100} are reached among pairs defined as category B. This observation underscores the relevance of the degree of sinuosity as a more informative factor than the value of the hypsometric integral alone. Changes in the shape of the hypsometric curve directly affect a watershed's snow accumulation capacity; basins with a high percentage of high elevation areas, associated with upward-convex curves (and low z values), would experience the largest changes due to warmer temperatures. Watersheds belonging to pairs 1, 3 and 4 clearly confirm this behavior, as those with higher Δq_{100} also have a greater percentage of high elevation areas (see Fig. 8 and Table 2). Although pair 5 may seem to contradict this pattern, it is important to note that the two curves cross each other, exactly at the highest elevations. While this detail is not immediately evident from Fig. 8, the curve for basin 180 lies above that of basin 183 for high values of $R_{elevation}$, before reversing for lower elevations. This explains why the larger Δq_{100} is observed for basin 180. Separate considerations are needed for pair number 2, whose basins exhibit hypsometric curves with absolutely comparable degrees of sinuosity. The difference in the Δq_{100} values they reach can likely be attributed to the difference in their maximum elevations, which is about 500 m.

The most interesting pairs identified (i.e. those having the lowest values of $d_{attributes}/d_{\Delta q}$) remain as such also when looking at the relative changes in the q_{10} quantile. Additional pairs emerge as potentially interesting in this case; however, these new pairs involve catchments identified as exceptions in section 4.1, which will be examined in detail in the following section.

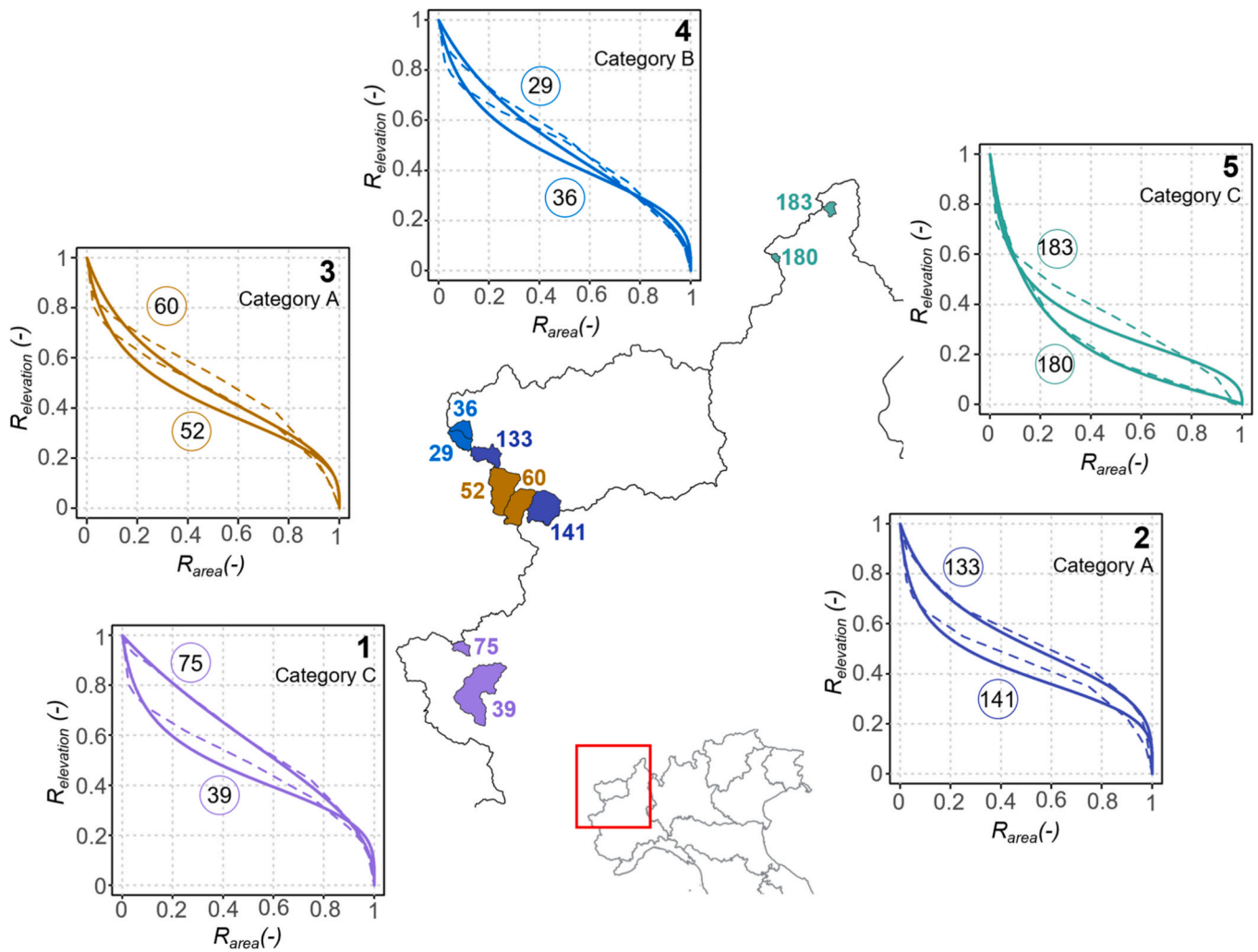


Fig. 8. Location and hypsometric curves of selected paired catchments. Dashed and solid curves represent the empirical hypsometric curves and those modeled with Strahler's function, respectively. Basin IDs are given in Table S1 in the Supplementary Material. $R_{elevation}$ = relative elevation; R_{area} = relative area.

5. Discussion

5.1. Reference flood frequency curves

As explained earlier, the rates of increase in current flood quantiles

have been calculated using a runoff coefficient $C = 1$ for all catchments. However, this section presents a calibration example of the C values to evaluate the model's ability in reproducing empirical FFCs for high-elevation basins.

The calibration example provided here has been performed by

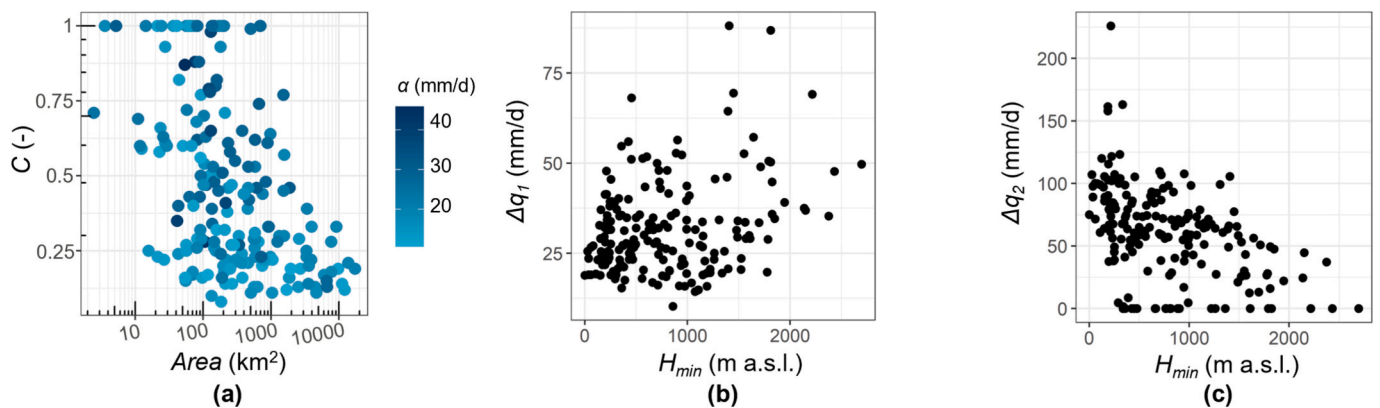


Fig. 9. Relationship between calibrated runoff coefficient (C) values and catchment areas and average values of daily extreme rainfall α (a); flood attenuation due to snow contribution (b) and infiltration losses (c) as functions of the minimum basin elevation H_{min} . Δq_1 is the distance between a 100-year return period rainfall quantile and the corresponding flood quantile recorded on the curve built with “uncalibrated” C ; Δq_2 is the distance between the flood quantiles measured on the “calibrated” and “uncalibrated” curves for the same 100-year return period.

forcing curves to match only one point, specifically the most extreme flood in the record. The variability of C values calibrated as described above on the 192 basins is depicted in Fig. 9a, in relation to the basin area and to the average rainfall intensity α . The values obtained are found to be plausible and somewhat consistent with the characteristics of the basins considered, since lower runoff coefficients are generally observed as the basin area increases and the average rainfall intensity decreases (this is described e.g. by Norbiato et al., 2009; Merz and Blöschl, 2009).

The values of Δq_1 and Δq_2 for 192 basins, computed according to Eqs. (3) and (4) for a return period of 100 years, are depicted as a function of the basin minimum elevation in Fig. 9b and 9c, respectively. The magnitude of flood attenuation due to the snow contribution (Δq_1) increases as the minimum basin elevation increases, while an opposite pattern is observed in the case of attenuation related to the effect of the runoff coefficient (Δq_2). This observation suggests that basins at higher elevations tend to exhibit more pronounced deviations in the shape of rainfall and flood frequency curves, confirming what was found by Claps and Laio (2004). Increasing values of Δq_1 with increasing minimum basin elevations confirm the larger impact of snow at higher elevations, which underscore the validity of *FloodAlp* as a tool for FFC estimation in mountain basins. The shape of the empirical FFC is, in fact, reasonably replicated in approximately 80 % of the catchments analyzed.

To quantify the model's accuracy in reproducing the shape of the empirical FFCs, the Kolmogorov-Smirnov distance (KS_d) is used. We calculate two KS_d values: one using the uncalibrated model curve and one using a calibrated curve, with the adjustment of C . The distribution of both KS_d values is depicted in Fig. 10a. Of course, the prediction accuracy improves considerably after calibrating the scaling factor, resulting in a much higher number of basins with smaller KS_d values. However, one can notice from Fig. 10b that the KS distance measured on the uncalibrated curve decreases for increasing minimum basin elevation for the majority of the catchments. These findings further support previous assessments of the model's suitability for applications in mountain regions.

5.2. Basin vulnerability to rising temperatures driven by elevation and hypsometry

Our study provides clear evidence that watershed elevation, particularly mean elevation, together with minimum elevation in the western Alps and maximum elevation in the eastern Alps, plays a crucial role in modulating the effects of global warming on both the 10-year and the 100-year floods in Alpine basins in Italy. This finding underscores the well-established understanding in the literature that watershed

elevation is a key factor in determining potential changes in flood magnitudes (e.g., Köplin et al., 2012; Fatichi et al., 2015; Chegwidan et al., 2020; Hanus et al., 2021; Moraga et al., 2021). Moreover, even if simplified assumptions are introduced in our analysis, *FloodAlp* produces results that are comparable to those from previous, more complex, studies (e.g. Köplin et al., 2012; Brunner et al., 2021).

Our findings also reveal different magnitudes of the rate of increase in small (10-year) vs. large (100-year) floods due to rising temperatures. With very few exceptions, Δq_{10} is consistently larger than Δq_{100} across the analyzed catchments for a given temperature scenario. This finding aligns well with the observation that extreme floods in the Alps typically occur during summer (Hall and Blöschl, 2018), when the active runoff-contributing area is already at or near its maximum extent. Consequently, for the 100-year flood, any further expansion of the contributing area due to warming appears to have a limited effect, whereas smaller floods remain more sensitive to temperature increases. Only a very small number of catchments within the Dora Baltea, Stura di Lanzo and Toce river basins, in the western and central Alps, exhibit an opposite behavior, with one of them showing negative Δq_{10} values (see Fig. 5b). These watersheds are all characterized by very high minimum elevations, exceeding 2500 m a.s.l., which means they remain almost always above the freezing level. As small floods do not exclusively occur during summer, but can also happen during colder periods of the year, when temperatures are still low, warming does not necessarily result in increased runoff.

Our research goes beyond the investigation of the role of watershed elevation, by demonstrating that, even at similar elevations, basin hypsometry is a key factor in determining the impacts of warming: apparently very similar watersheds, but having differing hypsometric features, exhibit quite different sensitivities to rising temperatures (see Fig. 8 and Table 2).

The influence of morphological characteristics on basin sensitivity to a snowline elevation increase, represented here using the hypsometric curve, is quite heterogeneous across the investigated areas. In the western Alps, the shape of the hypsometric curve plays a more significant role in affecting flood magnitude changes compared to other regions, where mean elevation is the main controlling factor. Our analysis reveals that the degree of sinuosity of the hypsometric curve can be a more robust predictor of both the 10-year and the 100-year flood sensitivity to rising temperatures than the hypsometric integral value, which represents the area under the curve.

This result further highlights the importance of the structural improvements made to the modeled hypsometric curve. Without these modifications, the substantial hypsometric differences between basins, such as those in pair n. 1, would have remained undetected, as

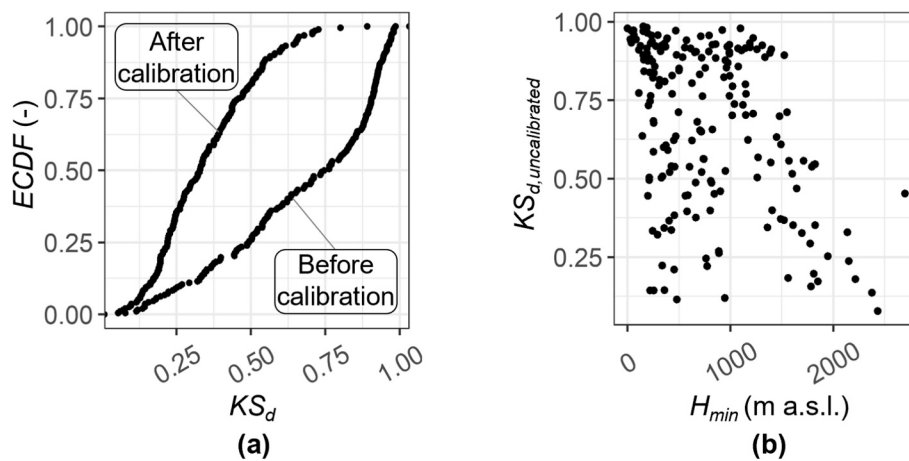


Fig. 10. Model's accuracy in reproducing empirical flood frequency curves. Empirical cumulative distribution functions ($ECDF$) of Kolmogorov-Smirnov distances (KS_d) measured both before and after calibration of the runoff coefficient (a); relationship between the Kolmogorov-Smirnov distance measured on the uncalibrated curve ($KS_{d, uncalibrated}$) and the minimum basin elevation (H_{min}) (b).

illustrated in Fig. 2. These differences are crucial for understanding how the Alpine catchments respond to temperature changes. The paired-catchment analysis that we have performed can therefore contribute to a larger-scale perspective, specifically highlighting the different vulnerability of the western Alps in comparison to the eastern Alps. This difference aligns with the evidence that the eastern Alps are characterized by the presence of carbonate rocks, mainly limestones and dolomites, which are highly susceptible to surface erosion (Gradwohl et al., 2024). This is likely to result in different hypsometric characteristics between the two compartments.

While the influence of catchment elevation is acknowledged in the literature, the role of the hypsometric curve has largely remained unexplored in the context of climate change-induced flood hazard. To the best of our knowledge, the only study where this characteristic is explicitly explored is that of Shea et al. (2021). However, our research extends their work by exploring this aspect further. We find that as the portion of the area at higher elevations increases (i.e. as the z parameter decreases), the change in the 100-year flood becomes more significant (see Fig. 6a). This finding represents a step forward from the previous study of Shea et al. (2021), who found that “bottom-heavy” basins (i.e. basins with a larger proportion of their area at low elevations, and with high z values, according to our scheme) are the most vulnerable to climate change in terms of snowpack volumes and melting timing. Some considerations are needed to understand what may appear as a contradictory finding. First, basins in southern Canada and northern USA, investigated by Shea et al. (2021), have average elevations not exceeding 1800 m a.s.l., and are typically covered by snow year-round. In contrast, the basins we considered in the Alps do not experience year-round snow cover. Second, different research objectives should be recognized between the two studies. The analysis performed by Shea et al. (2021) aims at estimating water resource availability, associated with areas that accumulate snow. Consequently, “bottom-heavy” basins are identified as the most vulnerable to rising temperatures in their work, as the snow accumulation would occur at low (and warmer) elevations. In contrast, our study focuses on the relevance of the opposite spatial domain, i.e. the basin area currently exposed to solid precipitation throughout the year, which makes basins with a high percentage of high elevation areas the ones that would experience the largest changes due to warmer temperatures.

Due to the complex heterogeneity and the current limitations in technical and scientific understanding of the processes involved, performing such a parsimonious analysis of the effects of climate change on natural hazards over large areas of the Alpine region could be perceived as overly simplistic. However, we do not consider this to be a significant limitation, as our aim is not to mandate precise instructions regarding the rate of increase in design flow rates. We also refrain from suggesting state-of-the-art methods for estimating design floods in a changing climate, for which additional research is still required. Our objective is to offer simple, yet clear, indications of mechanisms underlying potential changes in flood quantiles, focusing on the effects of rising temperatures, and describe the regions where the effects can be worse, to better inform decision-making about flood prevention and mitigation strategies.

If, with our arguments, we can agree with other authors in raising concern about the increasing flood hazard in high-elevation basins, our findings could help orientate land planners in prioritizing flood prevention measures based on the altitude and morphological characteristics of watersheds. Late spring and summer rainstorms in the Alps are already causing growing damages. However, mitigation strategies would benefit from a more differentiated approach, with the indications provided here, to prevent catastrophic (unprecedented) losses in environments with particularly vulnerable morphologies.

6. Conclusions

This research originates from the need to investigate which variables

have more influence on the natural processes that lead to floods from high elevation basins, and to figure out the potential effects caused by future variations in climatic conditions on the flood frequency regimes in mountain environments. The main contributions of this work are outlined as follows:

- i. a geomorphoclimatic methodology developed in 2009 has been considerably upgraded and implemented in a model named here *FloodAlp*. We managed to build conditions for a systematic application of the model over the entire Italian Alpine chain, which provides an unprecedented wide-area scenario of effects. To reproduce the basin hypsometric features, we introduce and assess the effectiveness of a two-parameter Strahler function, that yields results substantially different from those that would have been produced by the approach behind *FloodAlp* in its original form. These differences are stronger for basins with an empirical hypsometric curve exhibiting a pronounced double curvature;
- ii. we showed that the enhanced *FloodAlp* model can effectively serve diagnostic purposes by assessing the behavior of different types of high-elevation basins. To this end, the increase in the magnitude of “originary” 10-year and 100-year floods, has been obtained from the model as a result of projected gradual increases in the snowline elevation. Although not shown here, the model would also allow to simulate the effects of changes in the daily extreme rainfall or in the average number of rainfall events per year. Our approach is much simpler and parsimonious than existing studies, with no parameters to be fitted on recorded discharges to assess flood quantile changes. This makes our work more accessible and practical for the purpose of comparing the effects in different basins;
- iii. we found a pronounced responsiveness to rising temperatures above 2000 m a.s.l., with a potential increase of the current 10-year and 100-year floods of up to 18.5 % and 21 %, respectively, as a result of a 2 °C temperature rise. For a 4 °C increase in temperature, potential increases of 35 % and 43 % are found for the current q_{10} and q_{100} , respectively;
- iv. our analysis reveals that, particularly in the western Italian Alps, basin response to global warming is strongly controlled by the distribution of elevation within the basin, confirming the findings obtained in a previous study, where a more complex energy-balance model was used. Here, however, the relevant influence of local elevation conditions has been proved for a category of basins not previously investigated. Using a paired-catchment approach, we have shown how small variations in the degree of sinuosity of the basin’s hypsometric curve can lead to more than 50 % variations in the increase of the 100-year flood quantiles.

Funding

This study was carried out within the RETURN Extended Partnership and received funding from the European Union Next-GenerationEU (National Recovery and Resilience Plan – NRRP, Mission 4, Component 2, Investment 1.3 – D.D. 1243 2/8/2022, PE0000005 - Spoke TS 2).

CRedit authorship contribution statement

Giulia Evangelista: Writing – review & editing, Writing – original draft, Visualization, Validation, Software, Methodology, Investigation, Formal analysis, Data curation, Conceptualization. **Irene Monforte:** Writing – review & editing, Validation, Methodology, Formal analysis, Conceptualization. **Pierluigi Claps:** Writing – review & editing, Supervision, Resources, Methodology, Investigation, Funding acquisition, Formal analysis, Conceptualization.

Declaration of competing interest

The authors declare that they have no known competing financial interests or personal relationships that could have appeared to influence the work reported in this paper.

Acknowledgments

The authors wish to thank Marco Demateis Raveri for his valuable contribution to the data analysis.

Appendix A. Supplementary data

Supplementary data to this article can be found online at <https://doi.org/10.1016/j.jhydrol.2025.134014>.

Data availability

Results of this study are produced based on the methodology described in Allamano et al. (2009a). Data sources used are listed as follows: annual maxima of daily discharges and basin morphological parameters are retrieved from Claps et al. (2025), daily rainfall depths can be downloaded from the Archivio Climatologico per l'Italia Centro Settentrionale (data available at <https://www.arcsis.it/wp/en/products/upon> free registration), monthly mean rainfall depths can be downloaded from the BIGBANG dataset (available at <http://groupware.sinanet.isprambiente.it/bigbang-data/library/bigbang40>).

References

- Adler, C., Wester, P., Bhatt, I., Huggel, C., Insarov, G., Morecroft, M., Muccione, V., Prakash, A., Masson-Delmotte, V., Zhai, P., Pirani, A., Connors, S.L., Pean, C., Berger, S., Caud, N., Chen, Y., Goldfarb, L., Gomis, M.I., Huang, M., Leitzell, K., Lonnoy, E., Matthews, J.B.R., Maycock, T.K., Waterfield, T., Yeleki, O., Yu, R. & Zhou, B. (2022). *Contribution of Working Group II to the Sixth Assessment Report of the Intergovernmental Panel on Climate Change*. Cambridge: Cambridge University Press.
- Allamano, P., Claps, P., Laio, F., 2009a. An analytical model of the effects of catchment elevation on the flood frequency distribution. *Water Resour. Res.* 45, W01402. <https://doi.org/10.1029/2007WR006658>.
- Allamano, P., Claps, P., Laio, F., 2009b. Global warming increases flood risk in mountainous areas. *Geophys. Res. Lett.* 36, L24404. <https://doi.org/10.1029/2009GL041395>.
- Allamano, P. (2008). *Precipitation-runoff mechanisms in mountainous river basins*. Doctoral Dissertation. Torino, Italy: Politecnico di Torino.
- Avanzi, F., Gabellani, S., Delogu, F., Silvestro, F., Pignone, F., Bruno, G., Pulvirenti, L., Squicciarino, G., Fiori, E., Rossi, L., Puca, S., Toniazio, A., Giordano, P., Falzacappa, M., Ratto, S., Stevenin, H., Cardillo, A., Fioletti, M., Cazzuli, O., Cremonese, E., Morra di Cella, U., Ferraris, L., 2023. IT-SNOW: a snow reanalysis for Italy blending modeling, in situ data, and satellite observations (2010–2021). *Earth Syst. Sci. Data* 15, 639–660. <https://doi.org/10.5194/essd-15-639-2023>.
- Bajracharya, P., Jain, S., 2021. Characterization of drainage basin hypsometry: a generalized approach. *Geomorphology* 381, 107645. <https://doi.org/10.1016/j.geomorph.2021.107645>.
- Bavay, M., Grünewald, T., Lehning, M., 2013. Response of snow cover and runoff to climate change in high Alpine catchments of Eastern Switzerland. *Adv. Water Resour.* 55, 4–16. <https://doi.org/10.1016/j.advwatres.2012.12.009>.
- Blahušíková, A., Matoušková, M., Jeníček, M., Ledvinka, O., Kliment, Z., Podolinská, J., Snopková, Z., 2020. Snow and climate trends and their impact on seasonal runoff and hydrological drought types in selected mountain catchments in Central Europe. *Hydrol. Sci. J.* 65 (12), 2083–2096. <https://doi.org/10.1080/02626667.2020.1784900>.
- Blöschl, G., 2022. Three hypotheses on changing river flood hazards. *Hydrol. Earth Syst. Sci.* 26, 5015–5033. <https://doi.org/10.5194/hess-26-5015-2022>.
- Bongiovanni, G. (2025). *Assessment of climate change in the extended European Alpine region based on the novel EEAR-CLIM dataset* (Doctoral dissertation). IUSS Pavia, Italy.
- Brunner, M.I., Swain, D.L., Wood, R.R., et al., 2021. An extremeness threshold determines the regional response of floods to changes in rainfall extremes. *Commun. Earth Environ.* 2, 173. <https://doi.org/10.1038/s43247-021-00248-x>.
- Brunner, M.I., Farinotti, D., Zekollari, H., Huss, M., Zappa, M., 2019. Future shifts in extreme flow regimes in Alpine regions. *Hydrol. Earth Syst. Sci.* 23, 4471–4489. <https://doi.org/10.5194/hess-23-4471-2019>.
- Castellarin, A., Pistocchi, A., 2012. An analysis of change in alpine annual maximum discharges: implications for the selection of design discharges. *Hydrol. Process.* 26, 1517–1526. <https://doi.org/10.1002/hyp.8249>.
- Chegwidden, O.S., Rupp, D.E., Nijssen, B., 2020. Climate change alters flood magnitudes and mechanisms in climatically-diverse headwaters across the northwestern United States. *Environ. Res. Lett.* 15, 094048. <https://doi.org/10.1088/1748-9326/ab986f>.
- Braca, G., Bussetini, M., Lastoria, B., Mariani, S., & Piva, F. (2021). *Elaborazioni modello BIGBANG versione 4.0*, Istituto Superiore per la Protezione e la Ricerca Ambientale – ISPRA. Available at: <http://groupware.sinanet.isprambiente.it/bigbang-data/library/bigbang40>.
- Claps, P., Giordano, P., Laguardia, G., 2008. Spatial distribution of the average temperatures in Italy: quantitative analysis. *J. Hydrol. Eng.* 13 (4), 242–249. [https://doi.org/10.1061/\(ASCE\)1084-0699\(2008\)13:4\(242\)](https://doi.org/10.1061/(ASCE)1084-0699(2008)13:4(242)).
- Claps, P., Ganora, D., Evangelista, G., Mazzoglio, P., Bogoni, P., Demateis Raveri, M., & Monforte, I. (2025). *Catalogo delle Piene dei Corsi d'acqua Italiani Vol. 1*, 2^a Ed., Ed. CINID. In press.
- Confortola, G., Soncini, A., Bocchiola, D., 2014. Climate change will affect hydrological regimes in the Alps. *Journal of Alpine Research* 101. <https://doi.org/10.4000/rga.2176>.
- Diaz-Granados, M.A., Valdes, J.B., Bras, R.L., 1984. A physically based flood frequency distribution. *Water Resour. Res.* 20 (7), 995–1002. <https://doi.org/10.1029/WR020i007p00995>.
- Etter, S., Addor, N., Huss, M., Finger, D., 2017. Climate change impacts on future snow, ice and rain runoff in a Swiss mountain catchment using multi-dataset calibration. *J. Hydrol.: Reg. Stud.* 13, 222–239. <https://doi.org/10.1016/j.ejrh.2017.08.005>.
- Evangelista, G., Ganora, D., Mazzoglio, P., Pianigiani, F., Claps, P., 2023. Flood attenuation potential of Italian dams: sensitivity on geomorphic and climatological factors. *Water Resour. Manag.* 37 (15), 6165–6181. <https://doi.org/10.1007/s11269-023-03649-z>.
- Fatichi, S., Rimkus, S., Burlando, P., Bordoy, R., Molnar, P., 2015. High-resolution distributed analysis of climate and anthropogenic changes on the hydrology of an Alpine catchment. *J. Hydrol.* 525, 362–382. <https://doi.org/10.1016/j.jhydrol.2015.03.036>.
- Folton, N., Andréassian, V., Duperray, R., 2015. Hydrological impact of forest-fire from paired-catchment and rainfall-runoff modelling perspectives. *Hydrol. Sci. J.* 60 (7–8), 1213–1224. <https://doi.org/10.1080/02626667.2015.1035274>.
- François, B., Schlef, K.E., Wi, S., Brown, C.M., 2019. Design considerations for riverine floods in a changing climate – a review. *J. Hydrol.* 574, 557–573. <https://doi.org/10.1016/j.jhydrol.2019.04.068>.
- García-Valdecasas Ojeda, M., Di Sante, F., Coppola, E., Fantini, A., Nogherotto, R., Raffaele, F., Giorgi, F., 2022. Climate change impact on flood hazard over Italy. *J. Hydrol.* 615, 128628. <https://doi.org/10.1016/j.jhydrol.2022.128628>.
- Gradwohl, G., Stüwe, K., Liebl, M., Robl, J., Plan, L., Rummeler, L., 2024. The elevated low-relief landscapes of the Eastern Alps. *Geomorphology* 458, 109264. <https://doi.org/10.1016/j.geomorph.2024.109264>.
- Hall, J., Blöschl, G., 2018. Spatial patterns and characteristics of flood seasonality in Europe. *Hydrol. Earth Syst. Sci.* 22, 3883–3901. <https://doi.org/10.5194/hess-22-3883-2018>.
- Hanus, S., Hrachowitz, M., Zekollari, H., Schoups, G., Vizcaino, M., Kaitna, R., 2021. Future changes in annual, seasonal and monthly runoff signatures in contrasting Alpine catchments in Austria. *Hydrol. Earth Syst. Sci.* 25, 3429–3453. <https://doi.org/10.5194/hess-25-3429-2021>.
- Claps P., & Laio, F. (2004). *Peak over threshold analysis of flood and rainfall frequency curves*. Paper presented at ESF LESC Exploratory Workshop, Bologna, Italy.
- IPCC (2023). *Climate Change 2023: Synthesis Report*. In *Sixth Assessment Report of the Intergovernmental Panel on Climate Change* (35–115). Geneva, Switzerland: IPCC.
- Kemter, M., Merz, B., Marwan, N., Vorogushyn, S., Blöschl, G., 2020. Joint trends in flood magnitudes and spatial extents across Europe. *Geophys. Res. Lett.* 47, 7, e2020GL087464. <https://doi.org/10.1029/2020GL087464>.
- Köplin, N., Schädler, B., Viviroli, D., Weingartner, R., 2012. Relating climate change signals and physiographic catchment properties to clustered hydrological response types. *Hydrol. Earth Syst. Sci.* 16, 2267–2283. <https://doi.org/10.5194/hess-16-2267-2012>.
- Kreibich, H., et al., 2017. Adaptation to flood risk: results of international paired flood event studies. *Earth's Future* 5, 953–965. <https://doi.org/10.1002/2017EF000606>.
- Kundzewicz, Z.W., 2018. Quo vadis, Hydrology? *Hydrol. Sci. J.* 63 (8), 1118–1132. <https://doi.org/10.1080/02626667.2018.1489597>.
- Madsen, H., Rasmussen, P.F., Rosbjerg, D., 1997. Comparison of annual maximum series and partial duration series methods for modeling extreme hydrologic events: 1 At-Site Modeling. *Water Resour. Res.* 33 (4), 747–757. <https://doi.org/10.1029/96WR03848>.
- Mallucci, S., Majone, B., Bellin, A., 2019. Detection and attribution of hydrological changes in a large Alpine river Basin. *J. Hydrol.* 575, 1214–1229. <https://doi.org/10.1016/j.jhydrol.2019.06.020>.
- Meißl, G., Formayer, H., Klebinder, K., Kerl, F., Schöberl, F., Geitner, C., Markart, G., Leidinger, D., Bronstert, A., 2016. Climate change effects on hydrological system conditions influencing generation of storm runoff in small Alpine catchments. *Hydrol. Process.* 31 (6), 1314–1330. <https://doi.org/10.1002/hyp.11104>.
- Merz, R., Blöschl, G., 2009. A regional analysis of event runoff coefficients with respect to climate and catchment characteristics in Austria. *Water Resour. Res.* 45, W01405. <https://doi.org/10.1029/2008WR007163>.
- Moraga, J.S., Peleg, N., Fatichi, S., Molnar, P., Burlando, P., 2021. Revealing the impacts of climate change on mountainous catchments through high-resolution modelling. *J. Hydrol.* 603, 126806. <https://doi.org/10.1016/j.jhydrol.2021.126806>.
- Muelchi, R., Rössler, O., Schwanbeck, J., Weingartner, R., Martius, O., 2021. River runoff in Switzerland in a changing climate – runoff regime changes and their time of emergence. *Hydrol. Earth Syst. Sci.* 25, 3071–3086. <https://doi.org/10.5194/hess-25-3071-2021>.

- Norbiato, D., Borga, M., Merz, R., Blöschl, G., Carton, A., 2009. Controls on event runoff coefficients in the eastern Italian Alps. *J. Hydrol.* 375 (3–4), 312–325. <https://doi.org/10.1016/j.jhydrol.2009.06.044>.
- Ochoa-Tocachi, B.F., Buytaert, W., De Bièvre, B., 2016. Regionalization of land-use impacts on streamflow using a network of paired catchments. *Water Resour. Res.* 52, 6710–6729. <https://doi.org/10.1002/2016WR018596>.
- Pavan, V., Antolini, G., Barbiero, R., et al., 2019. High resolution climate precipitation analysis for north-central Italy, 1961–2015. *Clim. Dyn.* 52, 3435–3453. <https://doi.org/10.1007/s00382-018-4337-6>.
- Pike, R.J., Wilson, S.E., 1971. Elevation-relief ratio, hypsometric integral and geomorphic area altitude analysis. *Geol. Soc. Am. Bull.* 82 (4), 1079–1084. [https://doi.org/10.1130/00167606\(1971\)82\[1079:ERHIAG\]2.0.CO;2](https://doi.org/10.1130/00167606(1971)82[1079:ERHIAG]2.0.CO;2).
- Qixiang, W., Wang, M., Fan, X., 2018. Seasonal patterns of warming amplification of high-elevation stations across the globe. *Int. J. Climatol.* 38 (8), 3466–3473. <https://doi.org/10.1002/joc.5509>.
- Ragettli, S., Tong, X., Zhang, G., Wang, H., Zhang, P., Stähli, M., 2019. Climate change impacts on summer flood frequencies in two mountainous catchments in China and Switzerland. *Hydrol. Res.* 52 (1), 4–25. <https://doi.org/10.2166/nh.2019.118>.
- Rolland, C., 2003. Spatial and seasonal variations of air temperature lapse rates in alpine regions. *J. Clim.* 1032–1046. [https://doi.org/10.1175/15200442\(2003\)016%3C1032:SASVOA%3E2.0.CO;2](https://doi.org/10.1175/15200442(2003)016%3C1032:SASVOA%3E2.0.CO;2).
- Rottler, E., Vormoor, K., Francke, T., Warscher, M., Strasser, U., Bronstert, A., 2021. Elevation dependent compensation effects in snowmelt in the Rhine River Basin upstream gauge Basel. *Hydrol. Res.* 52 (2), 536–557. <https://doi.org/10.2166/nh.2021.092>.
- Scherrer, S., Gubler, S., Wehrli, K., Fischer, A.M., Kotlarski, S., 2021. The Swiss Alpine zero degree line: methods, past evolution and sensitivities. *Int. J. Climatol.* 41 (15), 6785–6804. <https://doi.org/10.1002/joc.7228>.
- Schneeberger, K., Dobler, C., Huttenlau, M., Stotter, J., 2015. Assessing potential climate change impacts on the seasonality of runoff in an Alpine watershed. *J. Water Clim. Change* 6, 263–277. <https://doi.org/10.2166/wcc.2014.106>.
- Shea, J.M., Whitfield, P.H., Fang, X., Pomeroy, J.W., 2021. The role of basin geometry in mountain snowpack responses to climate change. *Front. Water* 3, 604275. <https://doi.org/10.3389/frwa.2021.604275>.
- Sommer, C., Malz, P., Seehaus, T.C., et al., 2020. Rapid glacier retreat and downwasting throughout the European Alps in the early 21st century. *Nat. Commun.* 11, 3209. <https://doi.org/10.1038/s41467-020-16818-0>.
- Strahler, A.N., 1952. Hypsometric (area-altitude) analysis of erosional topography. *Geol. Soc. Am. Bull.* 63, 1117–1142.
- Tarasova, L., Lun, D., Merz, R., et al., 2023. Shifts in flood generation processes exacerbate regional flood anomalies in Europe. *Commun. Earth Environ.* 4, 49. <https://doi.org/10.1038/s43247-023-00714-8>.
- Wilhelm, B., Rapuc, W., Amann, B., et al., 2022. Impact of warmer climate periods on flood hazard in the European Alps. *Nat. Geosci.* 15, 118–123. <https://doi.org/10.1038/s41561-021-00878-y>.
- Zexia, C., Rui, Z., Zhenliang, Y., Qi, F., Linshan, Y., Lingge, W., Rui, L., Chunshuang, F., 2022. Hydrological response to future climate change in a mountainous watershed in the Northeast of Tibetan Plateau. *J. Hydrol.* 44, 101256. <https://doi.org/10.1016/j.ejrh.2022.101256>.